EXTERNAL REPORT
SCK•CEN-ER-242

Gamma dose assessment in near-range atmospheric dispersion simulations

Kevin Kenis
Ir. Lieven Vervecken
Dr. Johan Camps

August, 2013

SCK•CEN
Boeretang 200
BE-2400 Mol
Belgium

EXTERNAL REPORT OF THE BELGIAN NUCLEAR RESEARCH CENTRE
SCK•CEN-ER-242

Gamma dose assessment in near-range atmospheric dispersion simulations

Kevin Kenis
Ir. Lieven Vervecken
Dr. Johan Camps

August, 2013
Status: Unclassified
ISSN 1782-2335

SCK•CEN
Boeretang 200
BE-2400 Mol
Belgium

Studiecentrum voor Kernenergie
Centre d'étude de l'énergie Nucléaire
Boeretang 200
BE-2400 Mol
Belgium

Phone +32 14 33 21 11
Fax +32 14 31 50 21

http://www.sckcen.be

Contact:
Knowledge Centre
library@sckcen.be

Contents

1 Introduction

Simulation of the atmospheric dispersion of radioactive gases, released from a nuclear installation after an accident, and computation of the resulting dose rate, is an essential part of the nuclear emergency planning. It is in particular important in order to be able to take effective countermeasures. Although the existing (semi-)Gaussian models perform reasonably well in predicting the spatial distribution of the gas concentration at larger distance from the source, i.e. from a few hundred meters on, they have shown to be unreliable at closer range [Camps et al. (2010)]. The possibility of replacing these models at the near-range by a more accurate CFD model is therefore being investigated.

This work aims at implementing a gamma dose model in OpenFOAM, an open source CFD software package written in C++. OpenFOAM has an extensive range of features to solve anything from complex fluid flows involving chemical reactions, turbulence and heat transfer. The gamma dose model computes the dose rate at given locations based on dose-point-kernel approximation using a distributed simulated pollutant concentration as input.

This document is further organized as follows. First in Section 2, we present the dose-point-kernel approximation. In Section 3, we test and analyse the implemented model. Some case-studies are done in Section 4. In Section 5, we discuss the implementation. Finally, a summary can be found in Section 6.

2 Gamma dose model

The radioactive materials released into the atmosphere are transported according to the wind field over the terrain and dispersed over a wide area in an arbitrary form of distribution. The wind field is dependent on both geometrical and meteorological conditions. The exposure rate absorbed by a sensor on the ground due to the radioactive materials distributed in the air is calculated by following equation [Thykier-Nielson et al. (1995)]:

$$d(E_\gamma, C) = K\sigma_{en}E_\gamma \int_{x=-\infty}^{\infty}\int_{y=-\infty}^{\infty}\int_{z=0}^{\infty} \frac{B(\mu r)}{4\pi r^2} e^{-\mu r} C(x,y,z)\mathrm{d}x\,\mathrm{d}y\,\mathrm{d}z \quad (1)$$

where

d expected dose rate in a sensor [Gy/s]

K	constant, conversion factor, $1.6 \cdot 10^{-13}$ [Gy/s/MeV/kg]
σ_{en}	energy absorption coefficient for air [m^2/kg]
E_γ	energy of gamma radiation [MeV]
B	buildup factor
μ	linear attenuation factor for air [m^{-1}]
r	distance between the volume $dx\,dy\,dz$ and the sensor [m]
C	concentration at point (x, y, z) [Bq/m^3]

2.1 Buildup factor

There are many models available to approximate the buildup factor. For example: [Yoshida (2006)]

$$\begin{aligned} B(E,r) &= 1 + \frac{(b-1)\cdot K^r(E,r)}{K(E,r)-1} \quad \text{for} \quad K \neq 1 \\ &= 1 + (b-1)\cdot r \quad \text{for} \quad K = 1 \end{aligned} \tag{2}$$

where

$$K(E,r) = c \cdot r^a + d \cdot \frac{\tanh(\frac{r}{X_k - 2} - \tanh(2))}{1 - \tanh(-2)} \tag{3}$$

or [Trubey (1966)]

$$B(\mu, \mu_a, r) = 1 + k \cdot \mu \cdot r \tag{4}$$

$$k = \frac{\mu - \mu_a}{\mu_a} \tag{5}$$

The model used in this research [Taylor (1954)] is the following:

$$B(b) = Ae^{-\alpha_1 b} + (1-A)e^{-\alpha_2 b} \tag{6}$$

Where b is computed as μr and A, α_1, α_2 are model parameters which depend on E_γ. Values for these parameters are found in Table 5 in the appendix [Shure and Wallace (1988)]. A fit through this data has been performed and yields to following degree 6 polynomials.

$$\begin{aligned} \alpha_1(E) = &- 8.46767 \cdot 10^{-5}\tilde{E}^6 + 2.71806 \cdot 10^{-4}\tilde{E}^5 + 2.93831 \cdot 10^{-3}\tilde{E}^4 - \\ &6.30793 \cdot 10^{-3}\tilde{E}^3 - 1.84327 \cdot 10^{-2}\tilde{E}^2 + 4.78301 \cdot 10^{-2}\tilde{E} - \\ &4.61222 \cdot 10^{-2} \end{aligned} \tag{7}$$

With a coefficient of determination $R^2 = 0.968081$, and

$$\begin{aligned} \alpha_2(E) = &- 7.15631 \cdot 10^{-4}\tilde{E}^6 - 2.54597 \cdot 10^{-3}\tilde{E}^5 + 9.31948 \cdot 10^{-3}\tilde{E}^4 + \\ &1.89129 \cdot 10^{-2}\tilde{E}^3 - 3.12917 \cdot 10^{-2}\tilde{E}^2 + 1.49122 \cdot 10^{-2}\tilde{E} - \\ &1.02463 \cdot 10^{-2} \end{aligned} \tag{8}$$

With a coefficient of determination $R^2 = 0.963788$, where

$$\tilde{E} = \ln(E) \tag{9}$$

Figures of these fits are added to the appendix as figure 13 and figure 14 respectively.

For parameter A a good polynomial fit was not possible, so instead for each energy the A value corresponds to the energy which is closest to the listed energy value.

2.2 Linear attenuation factor

For the linear attenuation factor in air is no exact analytical formula available. Once again a polynomial fit of degree 6 has been performed through experimental data [ANS (1992)]. The data is shown in table 6 in the appendix. The polynomial fit is the following:

$$\begin{aligned}\mu(E) = &\exp(-1.40465 \cdot 10^{-4}\tilde{E}^6 + 3.07113 \cdot 10^{-4}\tilde{E}^5 + 1.42298 \cdot 10^{-2}\tilde{E}^4 - \\ &3.57795 \cdot 10^{-3}\tilde{E}^3 - 1.18921 \cdot 10^{-1}\tilde{E}^2 - 4.20821 \cdot 10^{-1}\tilde{E} - \\ &2.70365)/10 \cdot 1.2041\end{aligned} \tag{10}$$

With a coefficient of determination $R^2 = 0.990387$, where

$$\tilde{E} = \ln(E) \tag{11}$$

The division by 10 is to convert the units from [cm^2/g] to [m^2/kg]. In addition, in order to obtain μ one has to divide by the density of air, which is 1.2041 kg/m^3 at 20 $^\circ C$ and 1 atmosphere. A figure of this fit is available in the appendix, figure 15.

The parameter R^2 is sufficiently high to expect a really good fit. It should be kept in mind however that this fit is derived for $\ln(\frac{\mu}{\rho})$. Taking the exponential of small error may lead to bigger errors. In table 1 are the relative errors shown with respect to the tabulated values. So the fitted values are

	μ
average	0.0901
std dev	0.0662
max	0.2592

Table 1: Relative error of μ

not as good as might be expected by looking at R^2, the major problem is for low energies. This is illustrated in table 2 where the relative error for energies bigger then 0.080 MeV is computed.

	μ
average	0.0536
std dev	0.0352
max	0.1312

Table 2: Relative error of μ from 0.080 MeV upwards

2.3 Energy absorption coefficient

Like the linear attenuation factor, no exact analytical expression is available to calculate the energy absorption coefficient in air. So just as before a polynomial fit through experimental data [ANS (1992)] has been performed. In order to get a good fit, the data has been split in two parts. A 5th and 6th degree polynomial has been fit through both parts respectively. The data is shown in table 6 in the appendix. The fit is the following:

$$\sigma_{en}(E) = \begin{cases} \exp(-9.27823 \cdot 10^{-3}\tilde{E}^5 + 2.62726 \cdot 10^{-1}\tilde{E}^4 + \\ 2.92391\tilde{E}^3 + 1.58909 \cdot 10^{1}\tilde{E}^2 + 3.89774 \cdot 10^{1}\tilde{E} + \\ 3.06711 \cdot 10^{1})/10 & : E < 0.1 \\ R^2 = 0.999959 \\ \exp(1.06134 \cdot 10^{-5}\tilde{E}^6 - 1.59201 \cdot 10^{-3}\tilde{E}^5 + \\ 7.51537 \cdot 10^{-3}\tilde{E}^4 + 2.35368 \cdot 10^{-2}\tilde{E}^3 - \\ 1.19158 \cdot 10^{-1}\tilde{E}^2 - 1.82464 \cdot 10^{-1}\tilde{E} - \\ 3.57954)/10 & : E \geq 0.1 \\ R^2 = 0.999961 \end{cases} \tag{12}$$

where

$$\tilde{E} = \ln(E) \tag{13}$$

The division by 10 is once again to convert the units from $[cm^2/g]$ to $[m^2/kg]$. A figure of this fit is found in the appendix, figure 16.

2.4 Discretization

In order to compute the dose, the concentration needs to be integrated over the full domain (cfr. Eq. 1). Because the concentration is computed in a discrete number of points over the whole domain, due to the finite volume approach OpenFOAM employs, this can be readily achieved by summing up the contributions of each cell individually.

$$d(E_\gamma, C) = K\sigma_{en}E_\gamma \sum_i \frac{B(\mu r_i)}{4\pi r_i^2} e^{-\mu r_i} C_i V_i \tag{14}$$

Where C_i is the concentration in cell i $[Bq/m^3]$, Vi the volume of cell i $[m^3]$ and r_i the distance between the sensor and the cell-center of cell i $[m]$. Hence, the assumption is made that each cell can be treated as a point source. See figure 1 for a sketch of the situation.

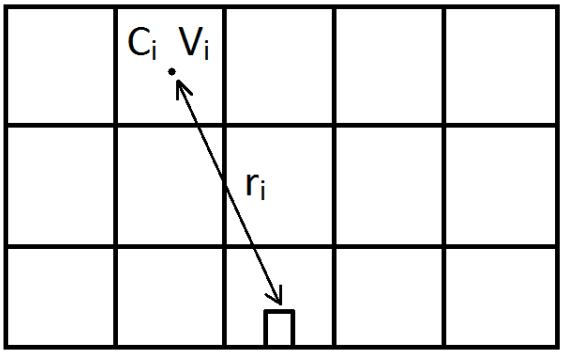

Figure 1: Disretization scheme

3 Testing and analyzing the model

3.1 Complexity

Lets first look at how the number of sensors and the number of cells in our mesh affects the computation time. It turns out that the computation time is linear with both the number of sensors and the number of cells in the mesh when keeping the other one constant.

3.2 Comparison with Nucleonica

The implementation of this model has been compared with data from the online nuclear science portal *Nucleonica* [Magill et al. (1959)]. Three isotopes have been studied, i.e. Argon-41, Vanadium-52 and Xenon-133. Figure 2 shows the comparison.

The calculated values for Argon-41 and Vanadium-52 match very well with the data from Nucleonica, with relative errors of less than 5% over the range examined. For Xenon-133 the values are less accurate. This is most likely

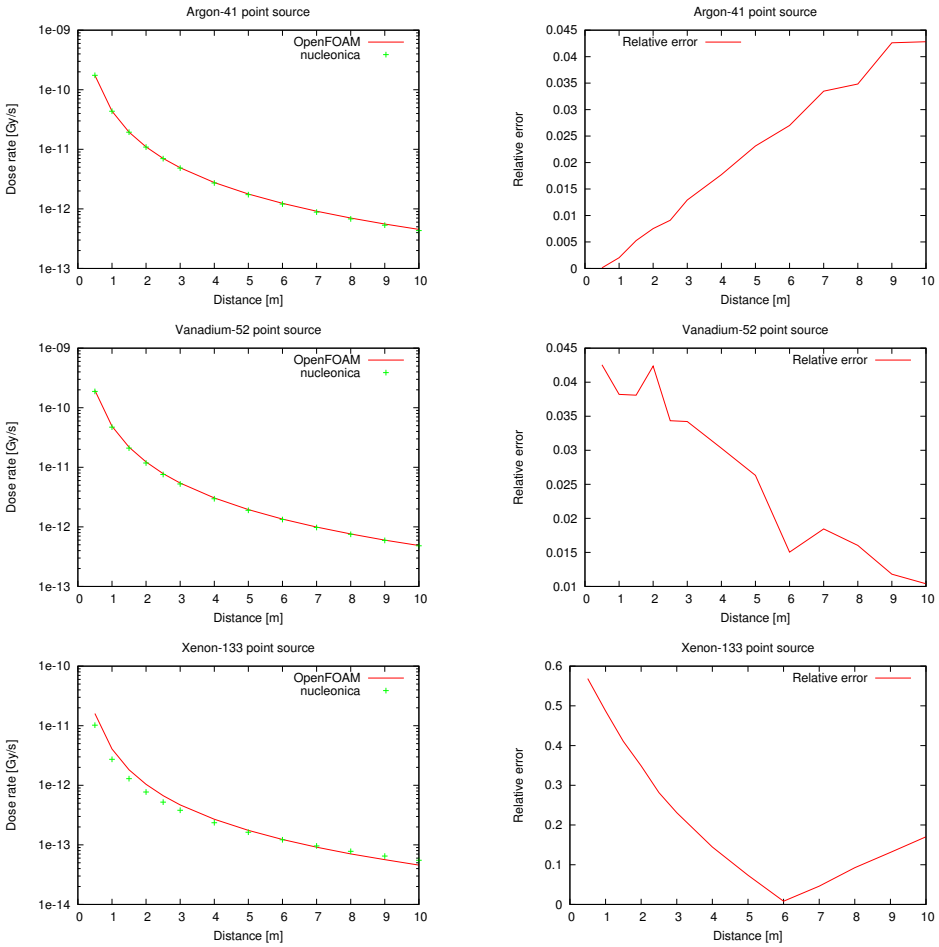

Figure 2: Comparison between nucleonica and model in OpenFOAM

due to the lower radiation energy. Because for the lower energies the fits needed for the buildup factor are less accurate, as mentioned in section 2.2.

3.3 Domain dependency

Since gamma rays are known to travel long distances, it is important to test if the dimensions of the used domain is important. This test is done for a cell size, the only thing that changes is the size of the domain. The dimensions of the domain vary from 1000×1000×500 to 2000×2000×500 m. A uniform concentration of 10^6 Bq is assumed. The test is done for a high and low energy pollutant, i.e. Argon-41 ($E_\gamma = 1.294$) and Xenon-133 ($E_\gamma = 0.081$). See figure 3.

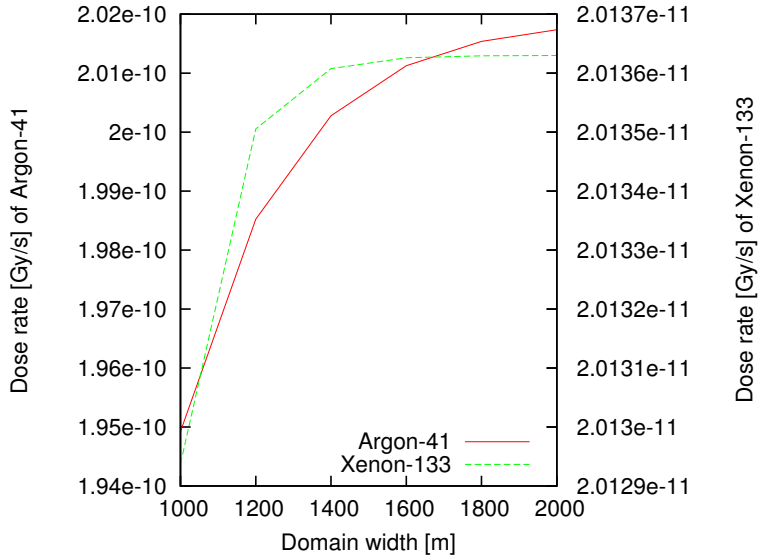

Figure 3: Domain width dependency of Argon-41 and Xenon-133

A bigger domain is needed for the higher energetic pollutants, which corresponds to them traveling further.

A second thing to test is the minimal allowable cell size for an accurate solution. The test is performed using a mesh of size $500 \times 500 \times 500$ m. The concentration has been put uniformly over the domain. The sensors (121 points) are placed uniformly between following points, $(200, 200, 1.5)$, $(200, 300, 1.5)$, $(300, 200, 1.5)$ and $(300, 300, 1.5)$.

On the x-axis of figure 4 is the number of cells in both x- and y-direction is shown. Something peculiar happens for x-values 50, 55, 100 and 105. Note that 55 and 105 is supposed to be 51 and 101, but plotted there for esthetic's. 2 observations can be made:

1. larger standard deviation for 51 and 101 and also a different average
2. smaller standard deviation for 50 and 100

The reason for the larger standard deviation and different average is shown in figure 5. For 51 and 101 the average distance between the sensor and the closest cell center is significantly smaller than for the other measurements.

For 50 and 100 an other effect plays, because of the setup all the sensor are placed precisely in between 2 cell-centers. This yields in a smaller standard deviation because all main contributors to the dose (the cells closest to the sensor) are at equal distance from the sensor.

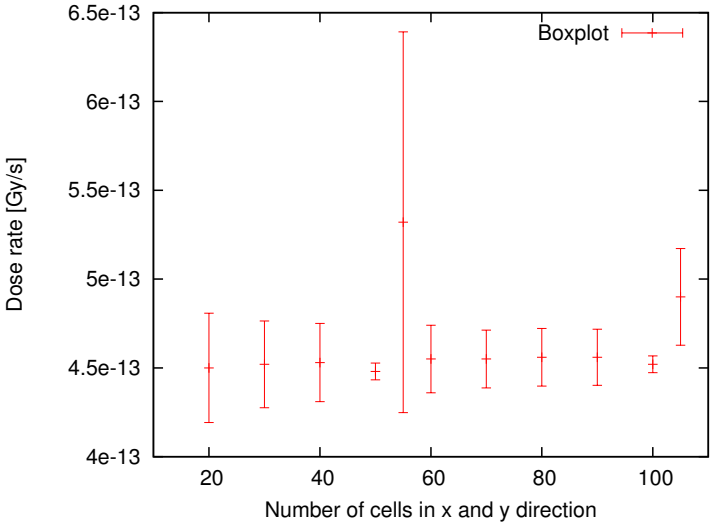

Figure 4: Boxplot of the dose rates for different number of cells

The most obvious conclusion would be to make sure not to put a sensor too close to a cell center. However, this turned out not to insufficient (see section 4.1) to address this issue.

4 Case-studies

4.1 Case 1: 20 meter tall chimney

This case-study concerns a constant release of a pollutant out of a 20 meter tall chimney. A 20 meter tall chimney has been chosen to limit the necessary domain for the calculations.

The pollutant dispersion behind the stack is simulated using the custom solver 'openfieldFoam'. This tool solves the convection-diffusion equation over an open field with uniform surface roughness. The analytical profiles for wind speed and diffusivity imposed, are derived from the Monin-Obukhov similarity theory [Vervecken et al. (2013)]. For the computational domain, we position the inlet boundary 250 m upstream of the source, and the outlet boundary 1750 m downwind from the source. Furthermore, the domain extends 400 m in each crosswind direction as seen from the source, and the height of the domain is set to 500 m. At the inlet, concentration is set to zero, at other boundaries Neumann boundary conditions are applied. The convection-diffusion equation is discretized on a Cartesian structured mesh consisting of 1.8M hexahedra, and employing second-order central schemes.

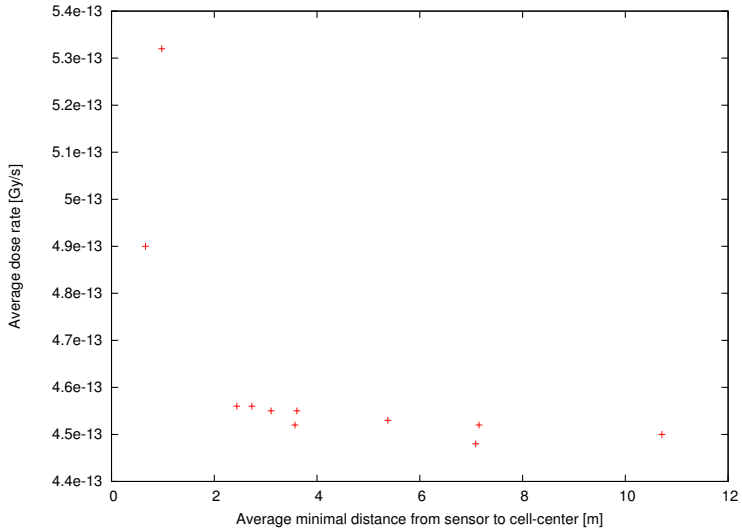

Figure 5: Dose rate dependency on sensor to cell distance

Height of chimney	20 m
u*	1.0 m/s^2
Windspeed at 20 m	19.002 m/s^2
Effective roughness height	0.01
Stability class	neutral ($L_{MO} = 10^{10}$)

Table 3: Parameters of simulation

Figure 6 shows the outline of the case, where the lines on the ground represent the placement of the sensors. In table 3 are all the parameters used in the openfieldFoam solver

Figure 7a shows the dose rates of the sensors that lie on the $y = 0$ axis and at ground level ($z = 0.01$).

The overall shape of the curve is expected, first there is a peak at certain distance after the chimney and then a drop of dose rate when going further away from the release point. This is because at first the cloud with the high concentration is further away and closes in with the distance, this results in the increase. Further on the cloud expands in the y-direction resulting in a decrease of the local concentration, this results in the decrease. The scatter on the other hand is not desired. This is caused by the sensor being to close to one or multiple cell centers. The reason why there is no scatter before a distance of approximately 100 meters is simply because the concentration

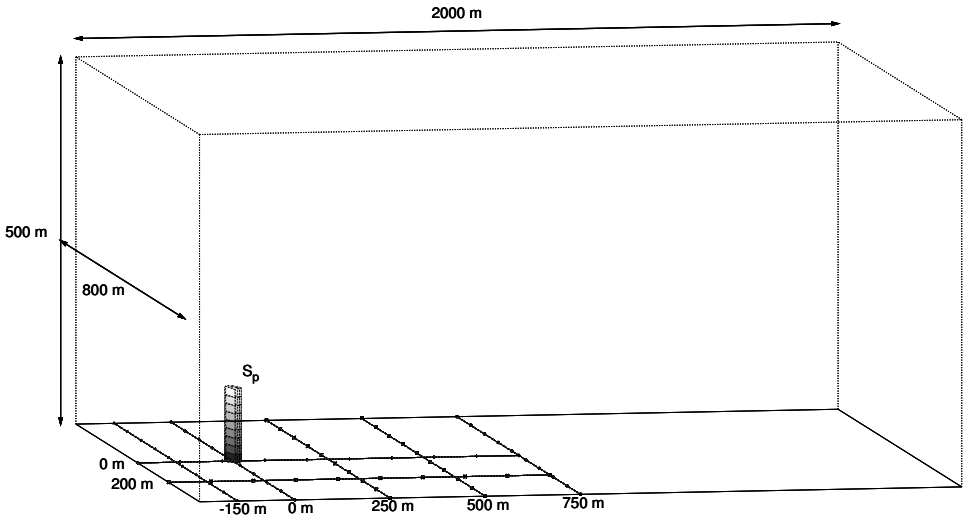

Figure 6: Outline of the case

in the cells near those sensors is practically zero, i.e. the main contributors to the dose are located at further distance from the sensor.

An initial attempt to solve this issue was to put the concentration in the cell where the sensor is located to zero. By doing this the contribution to the total dose rate of this cell is also put to zero. This leads to less scatter in the result, but it does not solve the issue, as shown in figure 7b.

Instead of setting the concentration in this specific cell to zero we also tried setting the concentration of the direct neighbors also to zero. This leads to figure 7c.

Again an improvement was obtained, but the level of scatter remains too high. In addition, setting the concentration to zero is also rather drastical. Therefore the dose rate coming from these cells should be calculated differently.

4.2 Uniform cloud approximation

In order to reduce the sensitivity of the result to the sensor positions, the idea is to work locally with a uniform cloud of concentration instead of multiple point sources. More specifically this means that we look at the dose rate coming from a uniform concentration cloud inside a hemisphere. This hemisphere is located around the sensor. Starting from this idea equation 1 becomes the following when changing the coordinate-system to a spherical one.

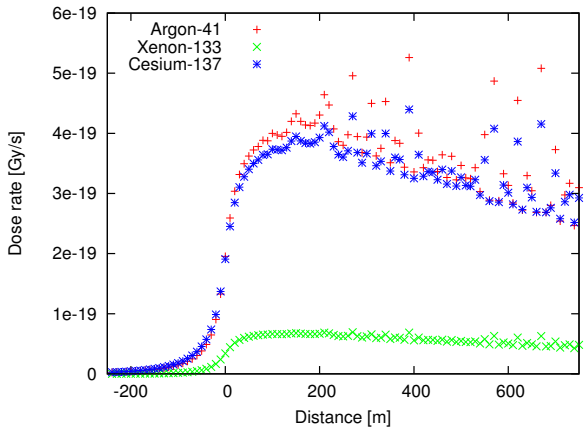

(a) All cells included

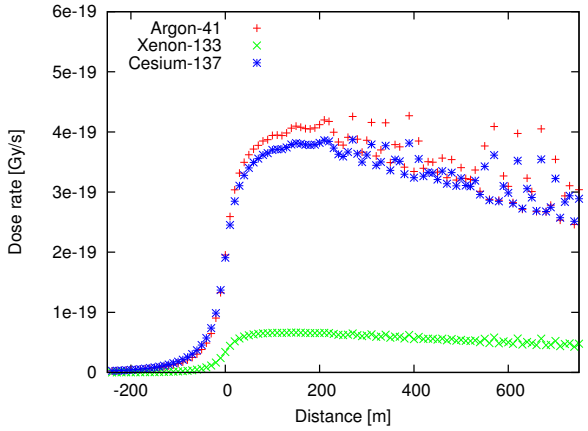

(b) Without cell that includes the sensor

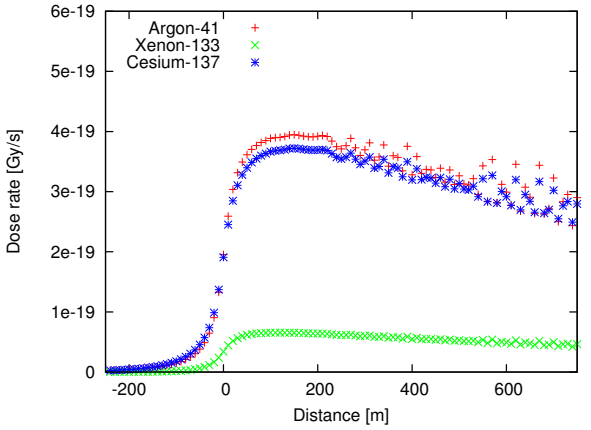

(c) Without cell that includes the sensor and without its neighbours

Figure 7: Comparison between nucleonica and model in OpenFOAM

$$d(E_\gamma, C) = \beta \int_{r=0}^{R} \int_{\theta=0}^{\frac{\pi}{2}} \int_{\phi=0}^{2\pi} \frac{B(\mu r)}{r^2} e^{-\mu r} \overline{C} r^2 \sin(\theta) \mathrm{d}r \, \mathrm{d}\theta \, \mathrm{d}\phi \tag{15}$$

$$= \beta 2\pi \overline{C} \int_{r=0}^{R} B(\mu r) e^{-\mu r} \mathrm{d}r \tag{16}$$

$$= \beta' \int_{r=0}^{R} A e^{-\alpha_1 \mu r - \mu r} + (1 - A) e^{-\alpha_2 \mu r - \mu r} \mathrm{d}r \tag{17}$$

$$= \beta' \left(\frac{A e^{-(\alpha_1+1)\mu R}}{-(\alpha_1+1)\mu} + \frac{(1-A) e^{-(\alpha_2+1)\mu R}}{-(\alpha_2+1)\mu} + \frac{A}{(\alpha_1+1)\mu} + \frac{1-A}{(\alpha_2+1)\mu} \right) \tag{18}$$

where

$$\beta' = 2\pi \overline{C} \beta \tag{19}$$

$$= 2\pi \overline{C} \frac{K}{4\pi} \sigma_{en} E_\gamma \tag{20}$$

$$= \overline{C} \frac{K}{2} \sigma_{en} E_\gamma \tag{21}$$

Because our implementation works in an discrete mesh we select all cells within a certain distance from the sensor and compute $\overline{C}$ as:

$$\overline{C} = \frac{\sum_i C_i \cdot V_i}{\sum_i V_i} \tag{22}$$

Where C_i and V_i are the concentration and volume of the selected cells. R is then determined as.

$$R = \sqrt[3]{\frac{3}{2\pi} \sum_i V_i} \tag{23}$$

4.3 Selecting the hemisphere radius

Previously we tried modifying the values corresponding to the cell, in which the sensor is located, and its neighbours. In most cases this will be enough, but this is strongly dependent on the size of the cells. That is why the selection criteria has been made dependent on the volume of the cell in which the sensor is located. We defined a characteristic length as follows:

$$L = \sqrt[3]{\tilde{V}} \tag{24}$$

Where $\tilde{V}$ is the volume of the cell in which the sensor is located. The selected cells are the ones who's cell-center is closer to the sensor then a specified number of times L. This specified number is to be chosen based on a few numerical experiments. Figure 8 shows this approach for various number of L on the case-study of the 20 meter tall chimney.

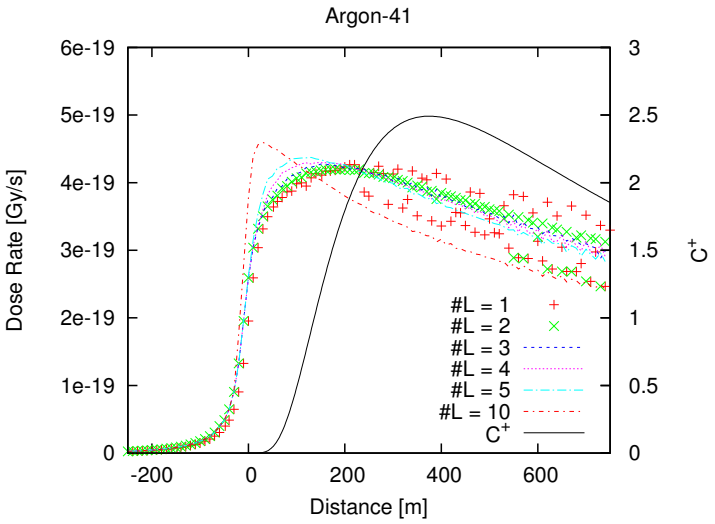

Figure 8: Sensor put on line under cloud axis

For this specific example 3 to 5 times the characteristic length L gives good smooth curves. However, increasing $\#L$ up to 10 shows a dependence of the result on this parameter. Here the curve gets more steep then for the other ones. This is not caused by the adjustment itself but because in this specific example our release-chimney is at 20 meters tall, and 10 characteristic lengths is more than 20 meters. This means that when applying the adjustment here you violate the uniform cloud approximation. A 20 meter high chimney is on the other hand rather small, in the next section a more representative case is studied.

Finally, note that the peak in dose rate is not at the same place as the peak of the concentration. The peak of the dose rate lies closer to the release point with respect to the peak of the concentration.

4.4 Case 2: 60 meter tall chimney

The situation is the same as for case 1, with the exception of the chimney height.

Let us first look at $\#L = 1$. Figure 9 shows plots for sensors put on several

Height of chimney	60 m
u*	1.0 m/s^2
Windspeed at 60 m	21.749 m/s^2
Effective roughness height	0.01
Stability class	neutral ($L_{MO} = 10^{10}$)

Table 4: Parameters of simulation

axes, e.g. $y = 0$ m, $x = 250$ m.

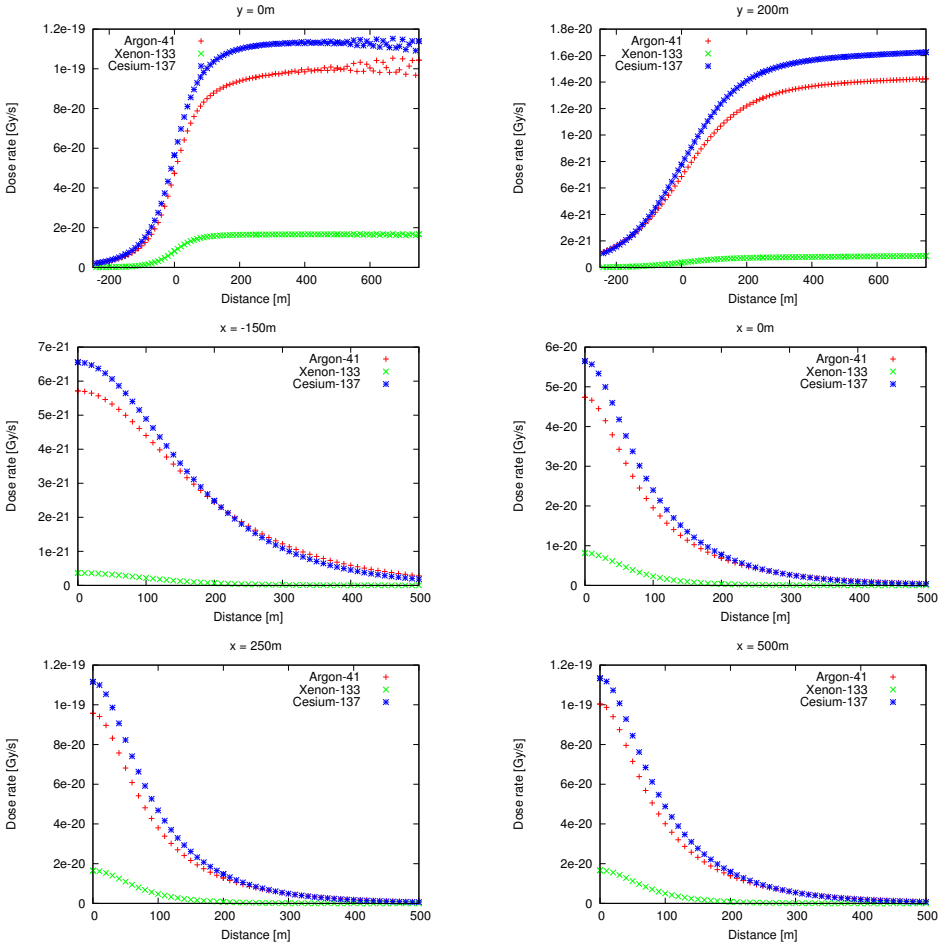

Figure 9: Cross sections for $\#L = 1$

The scatter problem is still visible, so we should take more then one characteristic length as threshold. It turned out that we should at least take $\#L = 4$ to smooth out all the curves, which can be seen in figure 10. Additionally, the effect of changing $\#L$ on the dose rate is plotted in figure

11.

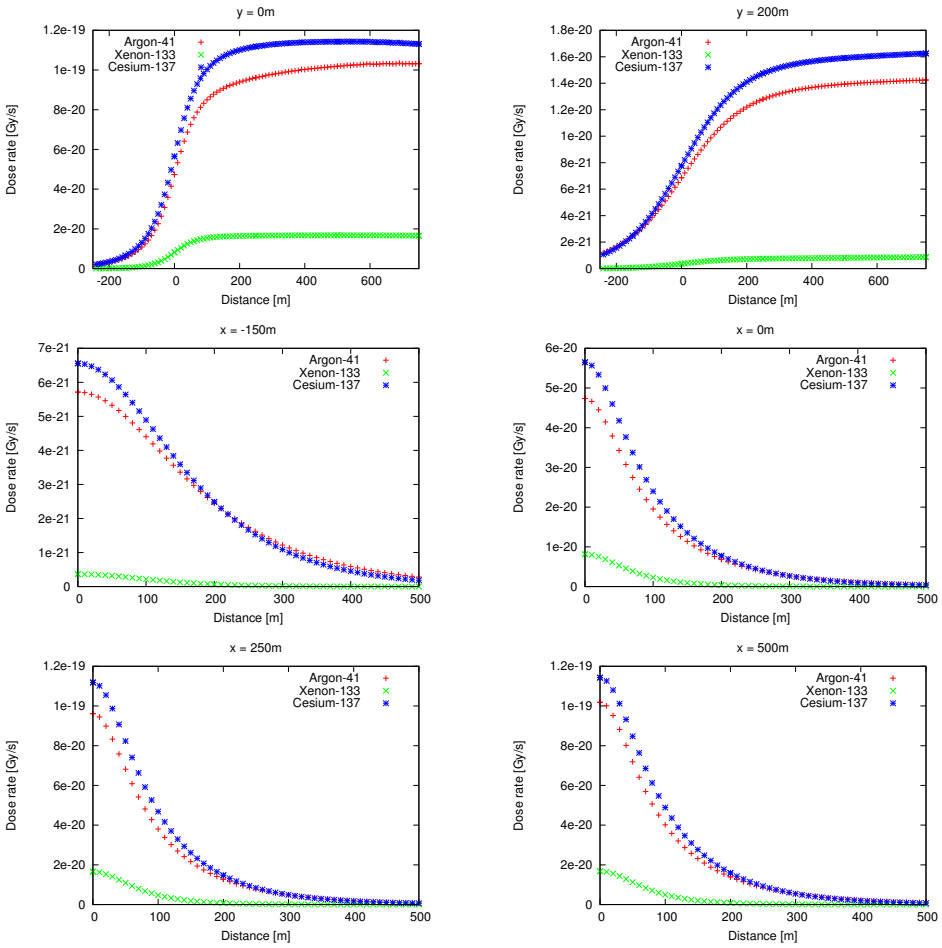

Figure 10: Cross sections for $\#L = 4$

When the chimney was 20 meters tall, the curve was more steep around zero. This is here not the case. Something else that can be seen is when $\#L$ increases, so does the dose rate. So the higher $\#L$ the more conservative the model is.

Another interesting fact is that the dose rate for Argon-41 was higher then the dose rate for Cesium-137 when the chimney was 20 meters tall. While now with the 60 meter tall chimney it is the other way around. The reason for this can be found in figure 12.

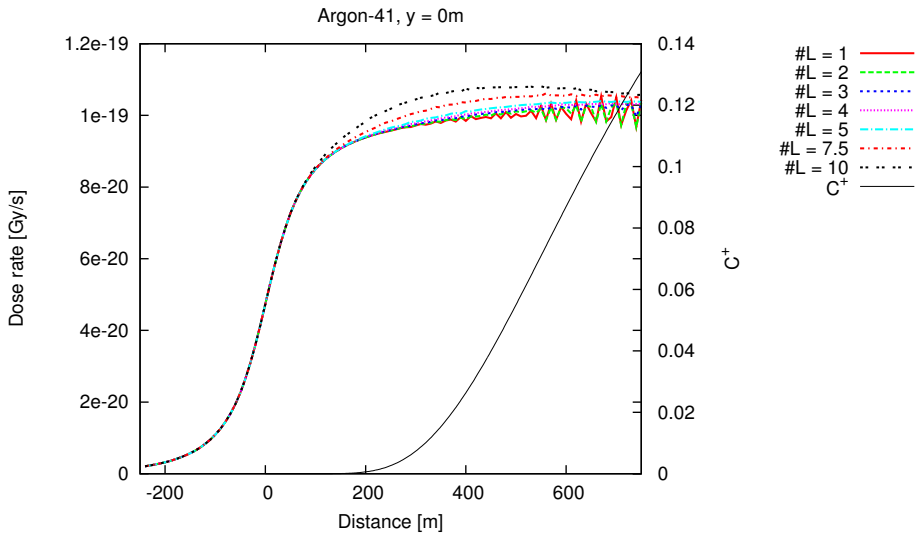

Figure 11: Cross section for multiple $\#L$

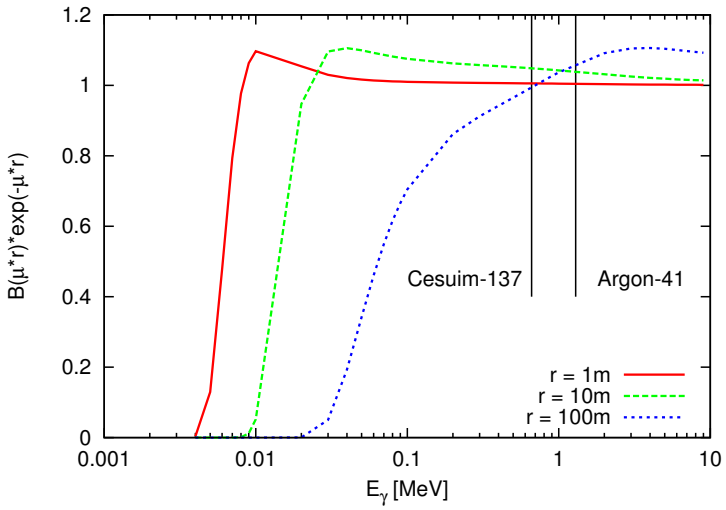

Figure 12: Buildup times exponential

One can see that it depends on the distance whether the factor increases or decreases with increasing the energy. In case 2 where the chimney was 60 meters tall, the higher concentration is further away from the ground then in case 1. At least for the first hundreds of meters after the chimney. This leads to a higher dose rate for Argon-41 in this case and a lower one in case 1.

5 Implementation

On the next page the class structure used in the implementation is shown. In this scheme one can see how the different classes are linked. Also this way of implementation leads to an easy extension possibility for alpha and beta decay. In addition the current implementation is fully parallelised and multiple pollutants, isotopes and time steps can be handled in a single run.

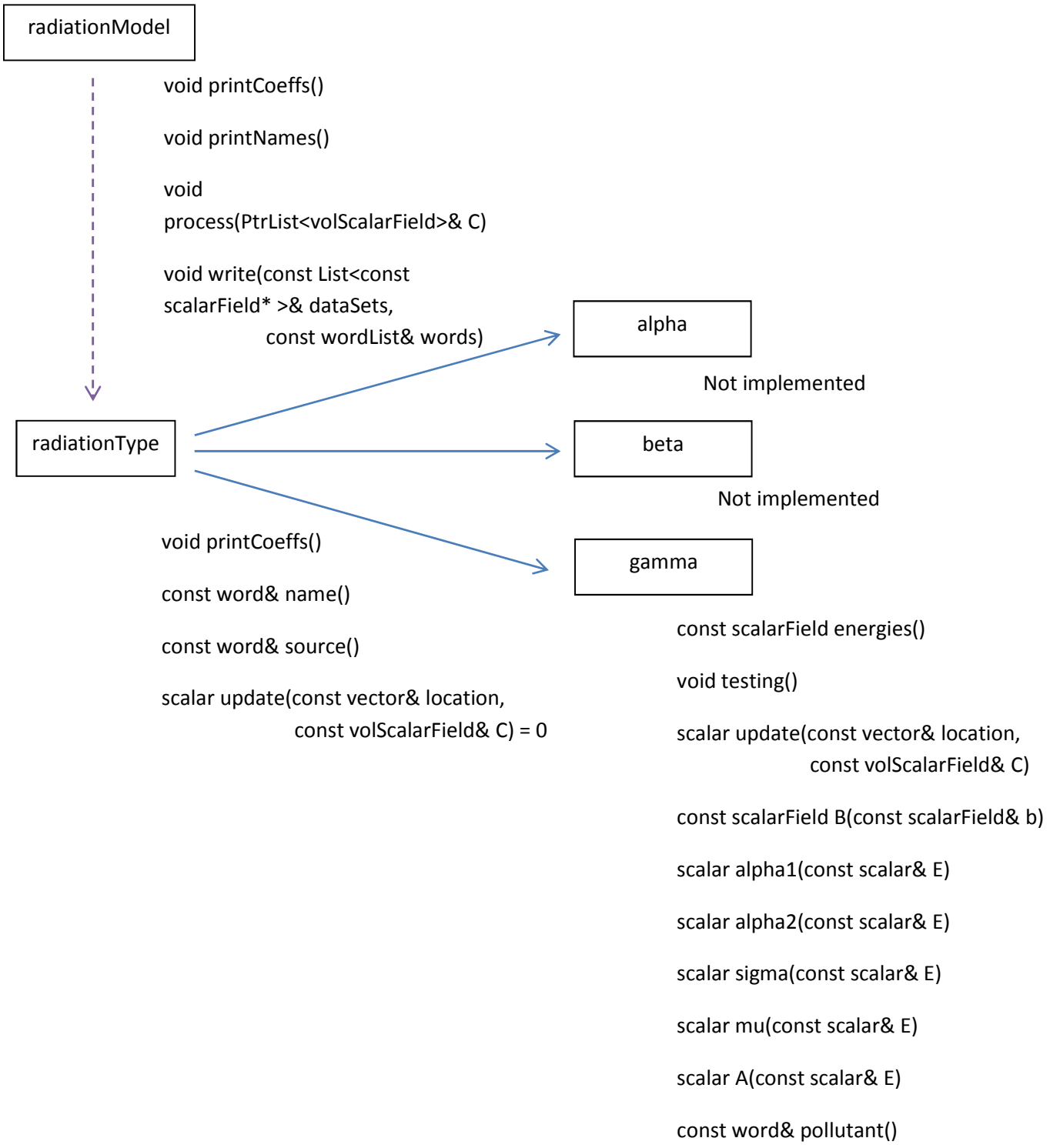
radiationModel
void printCoeffs()
void printNames()
void
process(PtrList<volScalarField>& C)
void write(const List<const
scalarField* >& dataSets,
const wordList& words)
radiationType
alpha
Not implemented
beta
Not implemented
gamma
void printCoeffs()
const word& name()
const word& source()
scalar update(const vector& location,
const volScalarField& C) = 0
const scalarField energies()
void testing()
scalar update(const vector& location,
const volScalarField& C)
const scalarField B(const scalarField& b)
scalar alpha1(const scalar& E)
scalar alpha2(const scalar& E)
scalar sigma(const scalar& E)
scalar mu(const scalar& E)
scalar A(const scalar& E)
const word& pollutant()

An input-file looks like this.

```
/*--------------------------------*- C++ -*----------------------------------*\
| =========                 |                                                 |
| \\      /  F ield         | OpenFOAM: The Open Source CFD Toolbox           |
|  \\    /   O peration     | Version:  2.0.1                                 |
|   \\  /    A nd           | Web:      www.OpenFOAM.com                      |
|    \\/     M anipulation  |                                                 |
\*---------------------------------------------------------------------------*/
FoamFile
{
    version     2.0;
    format      ascii;
    class       dictionary;
    location    "constant";
    object      radiationProperties;
}
// * * * * * * * * * * * * * * * * * * * * * * * * * * * * * * * * * * * * * //

printCoeffs    yes;
printLoc       yes;
testing        yes;

locations
    (
    (10 0 0.01)
    (20 0 0.01)
    );

write_dict
{
    format    gnuplot;
    dataName  doseRate;
    setName   pos1;
    axis      xyz;
}

radiation
(
    source0
    {
        pollutant          Argon-41;
        source             C0;
```

```
        E               1.294;
        dist            3;
        radiationType   gamma;
        printCoeffs     true;
    }

    source1
    {
        pollutant       Xenon-133;
        source          C0;
        E               0.081;
        dist            3;
        radiationType   gamma;
        printCoeffs     true;
    }

    source2
    {
        pollutant       Cesium-137;
        source          C1;
        E               0.662;
        dist            3;
        radiationType   gamma;
        printCoeffs     true;
    }
);

// ************************************************************************* //
```

6 summary

The method described is a good way to calculate the dose rate in a certain point coming from a cloud of pollutant. For point sources the implementation has been verified against the data from nucleonica. An initial test illustrated a strong dependence on the sensor location, resulting in large scatter on the estimated dose rates. By approximating the local concentration by a uniform cloud, this dependency has been tackled. The implementation of the model makes it possible to calculate the dose rate not only in a single point but in multiple points at the same time as well. It is even possible to calculate the dose rates for multiple pollutant at the same time. Furthermore it is possible to extend this model for α and β pollutants.

A Appendix

- Table 5: Parameters for buildup factor
- Table 6: Linear attenuation factor and energy absoption coefficient
- Figure 13: Fit for α_1
- Figure 14: Fit for α_2
- Figure 15: Fit for linear attenuation factor
- Figure 16: Fit for energy absorption coefficient

A.1 Tables

Energy[MeV]	A	α_1	α_2
0.015	1.585	-0.0032	0.2387
0.020	2.269	-0.0146	0.3247
0.030	6.729	-0.0380	0.2191
0.040	77.573	-0.0316	0.0001
0.050	179.362	-0.0624	-0.0374
0.060	142.500	-0.0975	-0.0506
0.080	218.520	-0.1237	-0.0854
0.100	615.000	-0.1237	-0.1096
0.150	148.122	-0.1450	-0.0940
0.200	401.090	-0.1237	-0.1096
0.300	159.500	-0.1096	-0.0801
0.400	90.000	-0.0975	-0.0562
0.500	69.409	-0.0871	-0.0417
0.600	70.160	-0.0759	-0.0387
0.800	109.832	-0.0532	-0.0341
1.000	86.171	-0.0444	-0.0243
1.500	59.400	-0.0312	-0.0107
2.000	32.192	-0.0271	0.0041
3.000	22.700	-0.0195	0.0151
4.000	11.638	-0.0230	0.0364
5.000	9.794	-0.0219	0.0366
6.000	9.568	-0.0179	0.0380
8.000	4.676	-0.0276	0.0766
10.000	5.059	-0.0215	0.0542
15.000	5.517	-0.0135	0.0366

Table 5: Parameters for buildup factor

Energy [MeV]	μ/ρ [cm^2/g]	σ_{en} [cm2/g]
1.00E-03	3.61E+03	3.60E+03
1.50E-03	1.19E+03	1.19E+03
2.00E-03	5.28E+02	5.26E+02
3.00E-03	1.63E+02	1.61E+02
3.20E-03	1.34E+02	1.33E+02
3.20E-03	1.49E+02	1.46E+02
4.00E-03	7.79E+01	7.64E+01
5.00E-03	4.03E+01	3.93E+01
6.00E-03	2.34E+01	2.27E+01
8.00E-03	9.92E+00	9.45E+00
1.00E-02	5.12E+00	4.74E+00
1.50E-02	1.61E+00	1.33E+00
2.00E-02	7.78E-01	5.39E-01
3.00E-02	3.54E-01	1.54E-01
4.00E-02	2.49E-01	6.83E-02
5.00E-02	2.08E-01	4.10E-02
6.00E-02	1.88E-01	3.04E-02
8.00E-02	1.66E-01	2.41E-02
1.00E-01	1.54E-01	2.33E-02
1.50E-01	1.36E-01	2.50E-02
2.00E-01	1.23E-01	2.67E-02
3.00E-01	1.07E-01	2.87E-02
4.00E-01	9.55E-02	2.95E-02
5.00E-01	8.71E-02	2.97E-02
6.00E-01	8.06E-02	2.95E-02
8.00E-01	7.07E-02	2.88E-02
1.00E+00	6.36E-02	2.79E-02
1.25E+00	5.69E-02	2.67E-02
1.50E+00	5.18E-02	2.55E-02
2.00E+00	4.45E-02	2.35E-02
3.00E+00	3.58E-02	2.06E-02
4.00E+00	3.08E-02	1.87E-02
5.00E+00	2.75E-02	1.74E-02
6.00E+00	2.52E-02	1.65E-02
8.00E+00	2.23E-02	1.53E-02
1.00E+01	2.05E-02	1.45E-02
1.50E+01	1.81E-02	1.35E-02
2.00E+01	1.71E-02	1.31E-02

Table 6: Linear attenuation factor and energy absorption coefficient

A.2 figures

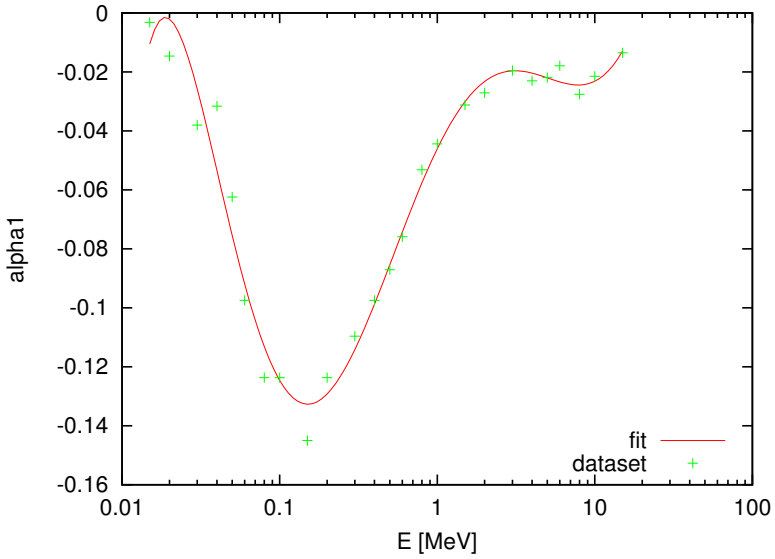

Figure 13: Fit for α_1

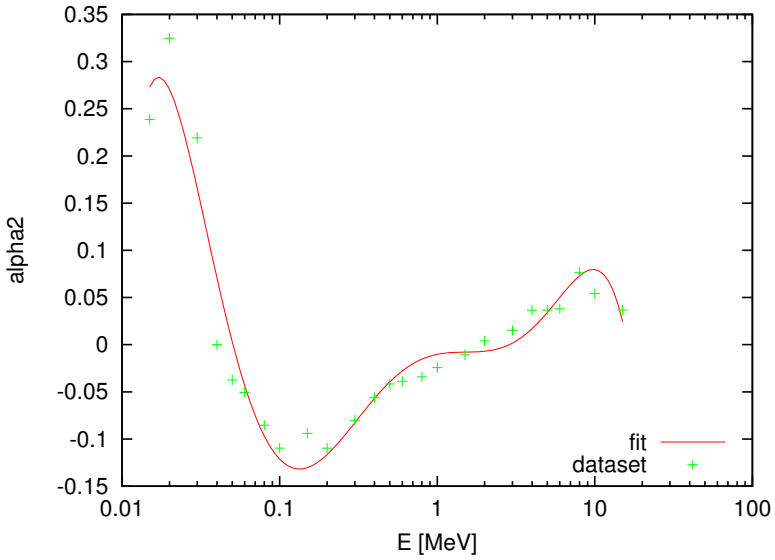

Figure 14: Fit for α_2

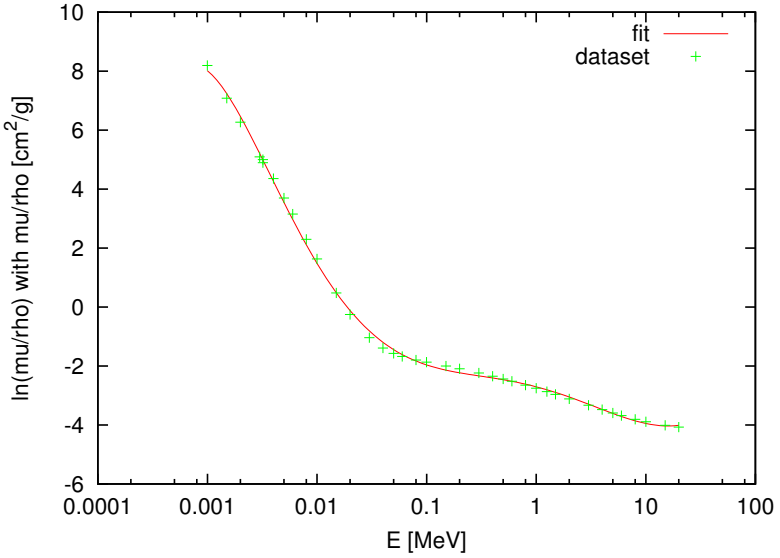

Figure 15: Fit for linear attenuation factor

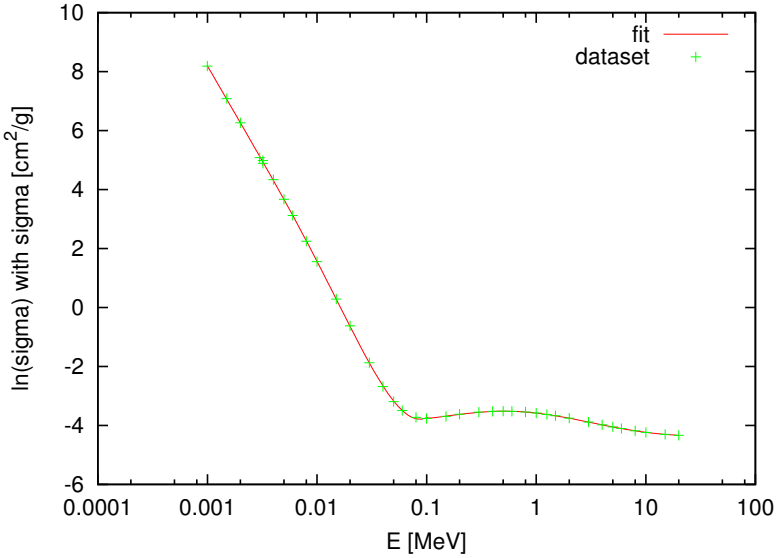

Figure 16: Fit for energy absorption coefficient

References

[ANS (1992)] Gamma-ray attenuation coefficients and buildup factors for engineering materials American Nuclear Society ANSI/ANS-6.4.3-1991.

[Brar et al. (1994)] Brar G. S., Sandhu A. K., Singh M., Mudahar G. S. 1994. Exposure Buildup Factors for Bakelite, Perspex and Magnox-A12 up to 40 mfp Using the Interpolation Method. Radiation Physics and Chemistry 44, 459–466.

[Camps et al. (2010)] Camps J., Turcanu C., Braekers D., Olyslaegers G., Paridaens J., e.a. 2010. The 'NOODPLAN' early phase nuclear emergency models: an evaluation. CD proceedings (also on-line available), Helsinki, Finland, 14-18 June 2010 / IRPA (International Radiological Protection Organization), Helsinki, Finland, IRPA.

[Cember and others (1969)] Cember H., 1969. Introduction to Health Physics. Pergamon Press Ltd..

[Han, Cho et al. (1995)] Han M. H., Cho G. S., Lee K. J. Chun M. H. 1995. Spherical Approximation in Gamma Dose Calculations and Its Application to an Emergency Response Action at Kori Reactor Site in Korea. Annals of Nuclear Energy 22, 441–452.

[Kurudirek and Özdemir (2011)] Kurudirek M., Özdemir Y. 2011. A Comprehensive Study on Energy Absorption and Exposure Buildup Factors for Some Essential Amino Acids, Fatty Acids and Carbohydrates i the Energy Range 0.015–15MeV up to 40 Mean Free Path. Nuclear Instruments and Methods in Physics Research Section B: Beam Interactions with Materials and Atoms 269, 7–19.

[Magill et al. (1959)] Magill J., Galy J., Dreher R., Hamilton D., Tufan M., Normand C., Schwenk-Ferrero A., Wiese H.W., 2007. NUCLEONICA: a nuclear science portal.. ENS News.17

[McGinnies (1959)] McGinnies R. T., 1959. X-ray Attenuation Coefficients from 10 keV to 100 MeV. National Bureau of Standards Gaithersburg MD.

[Park et al. (2000)] Park W. J., Han M. H., Lee K. J. 2000. Analysis of the Distributional Effects of Radioactive Materials on External Gamma Exposure. Annals of Nuclear Energy 27, 659–671.

[Shure and Wallace (1988)] Shure K., Wallace O., 1988. Taylor parameters for gamma-ray buildup factors in the proposed American National Standard. Bettis Atomic Power Lab., West Mifflin, PA (USA).

[Taylor (1954)] Taylor J.J. 1954. Application of gamma ray build-up data to shield design. Westinghouse Electric Corp. Atomic Power Div., Pittsburgh.

[Thykier-Nielson et al. (1995)] Thykier-Nielsen S., Deme S., Lang E. 1995. Calculation Method for Gamma Dose Rates From Gaussian Puffs. Risø National Laboratory

[Trubey (1966)] Trubey DK., 1966. A survey of empirical functions used to fit gamma-ray buildup factors. Oak Ridge National Lab., Tenn.

[Trubey (1991)] Trubey DK., 1991. New Gamma-Ray Buildup Factor Data for Point Kernel Calculations: ANS-6.4.3 Standard Reference Data.

[Vervecken et al. (2013)] Vervecken L., Camps J., Meyers J. 2013. Effect of Wind Fluctiations on Near-range Atmospheric Dispersion Under Different Types of Thermal Stratification. Proceedings of the 15th International Conference on Harmonisation within Atmospheric Dispersion Modelling for Regulatory Purposes.

[Yoshiko (1993)] Yoshiko H., 1993. An Historical Review and Current Status of Buildup Factor Calculations and Applications. Radiat. Phys. Chem. 41, 631–672.

[Yoshida (2006)] Yoshida Y. 2006. Develpment of Fitting Methods Using Geometric Progresion Formulae of Gamma-ray Buildup Factors. Journal of Nuclear Sciences and Technology 43, 1446–1457.